Appl Phys B (2012) 106:127–134
DOI 10.1007/s00340-011-4700-3

Applied Physics B
Lasers and Optics

Power spectral density of self-mixing signals from a flowing Brownian motion system

H. Wang · J. Shen

Received: 28 March 2011 / Revised version: 14 June 2011 / Published online: 28 August 2011

Abstract An analytical expression for the power spectral density of the self-mixing signals from a flowing Brownian motion system irradiated by a focused Gaussian field is derived from the time autocorrelation function of the signals. The power spectral density is composed of two Voigt functions. An improved series summation method (SSM) is proposed to calculate the Voigt function. The characteristics of the power spectral density are analyzed according to the numerical results. The power spectral density can hopefully be used for measuring the flow velocity and the particle size.

1 Introduction

Laser feedback interferometry (LFI), which is also known as laser self-mixing interferometry, is an interferometric sensing technique based on the optical mixing of the field in the laser cavity with the weak field back-reflected or backscattered by a remote target. The feedback interferometry in class-B lasers has attracted much attention mainly because class-B lasers are much more sensitive to the perturbations from the outside world than the conventional gas lasers [1]. Recently this technique has been applied for the analysis of flowing Brownian motion system in which the particles move randomly due to the collisions with molecules of liquid (i.e. Brownian motion) and directionally due to the translational flow of liquid (i.e. translational motion) [2–12]. The schematic diagram of feedback interferometry with laser diode in flowing Brownian motion system is shown in Fig. 1. The light emitting from the laser hits the flowing Brownian particles and is scattered back into the laser cavity. This causes the periodic change of laser light output frequency, linewidth, threshold gain, and output power, all of which relate to the phase of the backscattering light. The standard internal monitoring photodiode (PD), which is built into the commercial laser diode (LD) package, can be utilized to detect the output power.

The first attempt to explain the effects of laser diode self-mixing interferometry with weak optical feedback was made by Lang and Kobayashi in 1980 [13]. Their model describes the evolution of the electric field in a single mode laser diode in the rate-equation limit and includes the influence of the optical feedback through a time-delayed field term with coupling strength. In our previous paper [14], the back-scattered field from particles is introduced into the feedback term of the Lang–Kobayashi rate equations. An expression of the time autocorrelation function (TACF) of the back-emitted power from the laser cavity was obtained which includes the information of particle size and the translational velocity of particles. The time autocorrelation function can be transformed into the power spectral density (PSD) which includes the same information of the TACF. So in principle both the particle size and the translational velocity of particles can be extracted from the PSD too. In fact, what is usually measured in the self-mixing interferometry is the PSD of the self-mixing signals. In this paper, an analytical expression of the PSD is derived from the TACF, which is composed of two Voigt functions. In order to calculate the Voigt function much faster and accurately, an improved series summation method (SSM) is introduced. Numerical results of the power spectral density are shown to study its dependence on different physical quantities.

H. Wang · J. Shen (✉)
University of Shanghai for Science and Technology,
Shanghai 200093, China
e-mail: jqshenk@163.com

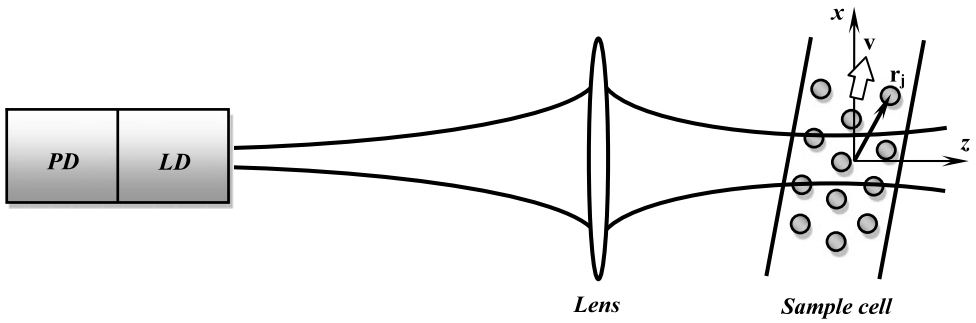

Fig. 1 Schematic diagram of feedback interferometry with laser diode in flowing Brownian motion system

2 Derivation of power spectral density

According to our previous work [14], the time autocorrelation function (TACF) of the output power from the laser cavity for a flowing Brownian motion system was obtained as

$$R(\tau) = P_0^2\Big\{1 + \underbrace{2m^2|C_{\mathrm{Mie}}|^2\langle N\rangle}_{\text{coefficient}}\underbrace{\cos(\mathbf{q}\cdot\mathbf{v}\tau)}_{\text{Dopplerterm}}\underbrace{\exp\big(-Dq^2\tau\big)}_{\text{Brownianterm}} \times \underbrace{\exp\big(-Q\tau^2\big)}_{\text{Gaussianterm}}\Big\} \tag{1}$$

where P_0 is the back-emitted power of laser diode in the absence of optical feedback; m is dependent on the characteristic parameters of the laser diode; $|C_{\mathrm{Mie}}|^2$ is related to the Mie solution of the Maxwell's equations for the scattering of electromagnetic radiation by spherical particles; $\langle N\rangle = N_T V_S/V_T$ is the average particle number located within the volume V_S; $\mathbf{q}$ is the scattering vector shown in Fig. 2, whose magnitude is given as $q = (4\pi\sin\theta/2)/\lambda$ with λ the light wavelength in medium and θ the scattering angle, $\mathbf{v}$ is the velocity of translational flow, ϕ the angle between the scattering vector and flow velocity; $Q = (v_x^2 + v_y^2)/2\omega_0^2 = v^2\sin^2\varphi/2\omega_0^2$ with $v_{x(y)}$ is the $x(y)$ component of the flow velocity vector $\mathbf{v}$, ω_0 is the beam waist radius; D is the diffusion coefficient given as $D = k_B T/3\pi\eta d$ with k_B the Boltzmann's constant, T the temperature, η the viscosity of suspension and d the particle diameter; the second term in (1) is a product of a Doppler shift term $\cos(\mathbf{q}\cdot\mathbf{v}\tau)$, a Brownian term $\exp(-Dq^2\tau)$ and a Gaussian term $\exp(-Q\tau^2)$. The Doppler shift term is due to the translational motion of particles, dependent on the magnitudes of the flow velocity, the scattering vector and the angle between them. The Brownian term is due to the diffusional motion of particles, dependent on the diffusion coefficient D and the magnitude of the scattering vector q. The Gaussian term depends on the translational motion of the particles through the Gaussian beam waist.

Since a signal with nonzero average power is not square integrable, the Fourier transform does not exist in this case.

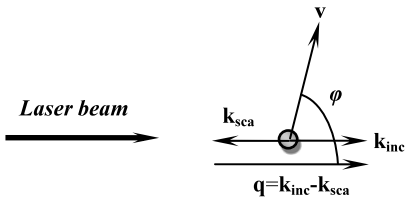

Fig. 2 Vector diagram of the scattering vector $\mathbf{q}$, the flow velocity $\mathbf{v}$ and the angle between them

Fortunately, the Wiener–Khinchin theorem provides a simple alternative. The PSD is the Fourier transform of the TACF of the signal as long as the signal can be treated as a wide-sense stationary random process. Thus, the PSD $S_0(\omega)$ is written as

$$S_0(\omega) \equiv F\big[R_0(\tau)\big] \equiv \int_{-\infty}^{\infty} R_0(\tau)e^{-i\omega\tau}\,d\tau \tag{2}$$

where ω is the angular frequency. According to the convolution theorem that the Fourier transform of a product of the factors is given by the convolution of the factors' Fourier transforms, (2) can be rewritten as

$$\begin{aligned} &F\big[R_0(\tau)\big] \\ &\quad = F\big[\exp\big(-Dq^2\tau\big)\exp\big(-Q\tau^2\big)\cos(\mathbf{q}\cdot\mathbf{v}\tau)\big] \\ &\quad = \frac{1}{2\pi}\frac{1}{2\pi}F\big[\exp\big(-Dq^2\tau\big)\big]\otimes F\big[\cos(\mathbf{q}\cdot\mathbf{v}\tau)\big] \\ &\qquad \otimes F\big[\exp\big(-Q\tau^2\big)\big] \end{aligned} \tag{3}$$

The Fourier transforms of the single factors in (3) are, respectively,

$$\begin{aligned} F\big[\exp\big(-Dq^2\tau\big)\big] &= \frac{2q^2D}{\omega^2 + (q^2D)^2} \\ F\big[\cos\mathbf{q}\cdot\mathbf{v}(\tau)\big] &= \pi\big[\delta(\omega + \mathbf{q}\cdot\mathbf{v}) + \delta(\omega - \mathbf{q}\cdot\mathbf{v})\big] \\ F\big[\exp\big(-Q\tau^2\big)\big] &= \sqrt{\frac{\pi}{Q}}\exp\Big[-\frac{\omega^2}{4Q}\Big] \end{aligned} \tag{4}$$

Substitution of (4) into (3) yields

$$F\left[\exp\left(-Dq^2\tau\right)\exp\left(-Q\tau^2\right)\cos(\mathbf{q}\cdot\mathbf{v}\tau)\right] = \frac{1}{2\pi}\sqrt{\frac{\pi}{Q}}\int_{-\infty}^{\infty}\left[\frac{q^2D\exp(-\omega'^2/4Q)}{(\omega'-\omega+\mathbf{q}\cdot\mathbf{v})^2+(q^2D)^2} + \frac{q^2D\exp(-\omega'^2/4Q)}{(\omega'-\omega-\mathbf{q}\cdot\mathbf{v})^2+(q^2D)^2}\right]d\omega' \tag{5}$$

With the substitutions of $\gamma_L = Dq^2$, $\gamma_G = 2\sqrt{Q\ln 2}$, $x_\pm = \sqrt{\ln 2}(\omega \pm \mathbf{q}\cdot\mathbf{v})/\gamma_G$, $y = \sqrt{\ln 2}\gamma_L/\gamma_G$ and $t = \sqrt{\ln 2}\omega'/\gamma_G$, we finally find the analytical expression of the PSD of the self-mixing signals:

$$S_0(\omega) = \frac{\sqrt{\pi\ln 2}}{\gamma_G}\left[\frac{y}{\pi}\int_{-\infty}^{\infty}\frac{\exp(-t^2)}{y^2+(x_+-t)^2}\,dt + \frac{y}{\pi}\int_{-\infty}^{\infty}\frac{\exp(-t^2)}{y^2+(x_--t)^2}\,dt\right] = \frac{\sqrt{\pi\ln 2}}{\gamma_G}\left[V(x_+,y)+V(x_-,y)\right] \tag{6}$$

where

$$V(x,y) = \frac{y}{\pi}\int_{-\infty}^{\infty}\frac{\exp(-t^2)}{y^2+(x-t)^2}\,dt \tag{7}$$

is the Voigt function. γ_L is the half-width for the Lorentzian broadening, γ_G is the half-width for the Gaussian broadening. Equation (6) is composed of two Voigt functions $V(x_\pm, y)$, one of which is centered at $\omega = \mathbf{q}\cdot\mathbf{v}$ and the other is centered at $\omega = -\mathbf{q}\cdot\mathbf{v}$. The profile of the Voigt function is a line profile resulting from the convolution of two mechanisms, one of which alone produces the Gaussian profile, and the other produces the Lorentzian profile.

3 Calculation of the Voigt function

Direct calculation of the integration of Voigt function is difficult. This is because that the Voigt function is the improper integral with both limits infinite and the integrand with the narrow peak makes the evaluation of any proper integral low efficiency and low precision. So, instead of the direct calculation of the integration, a lot of methods have been proposed to evaluate the Voigt function. To our knowledge, the method derived by Limandri et al. is one of the most accurate and fast ones for the evaluation of the Voigt function [15]. This method is called as series summation method (SSM) in our paper because the Voigt function is expanded finally as the series summation.

According to reference [15], the Voigt function is expressed in terms of the series approximation for the error function as

$$V(x,y) = \exp(-x^2)\left\{\operatorname{erfc}(y)\exp\left(y^2\right)\cos(2xy) + \frac{1}{2\pi y}\left(1-\cos(2xy)\right) + \frac{2}{\pi}\sum_{n=1}^{N}\frac{\exp(-n^2/4)}{n^2+4y^2}\left[g_n(x,y)\sin(2xy) - f_n(x,y)\cos(2xy)\right]\right\} \tag{8}$$

where

$$f_n(x,y) = 2y - 2y\cosh(nx)\cos(2xy) + n\sinh(nx)\sin(2xy)$$
$$g_n(x,y) = 2y\cosh(nx)\sin(2xy) + n\sinh(nx)\cos(2xy) \tag{9}$$

and the product $\operatorname{erfc}(y)\cdot\exp(y^2)$ used in (8) is evaluated according to the algorithm proposed by Cody [16]. The series summation, for each y, is truncated at the Number N:

$$N = \begin{cases} 15, & [0,3] \\ 50, & (3,20] \\ 110, & (20,50] \\ 150, & (50,75] \end{cases} \tag{10}$$

When $x > 75$, the Voigt function is computed numerically using the asymptotic expansion given by Roco and Téllez [17]:

$$V(x,y) \approx \frac{y}{\sqrt{\pi}(x^2+y^2)}\times\left[1-\frac{\cos(3\arctan\frac{x}{y})}{2(x^2+y^2)\cos(\arctan\frac{x}{y})}\right] \tag{11}$$

It is worth to point out that a high precision can be obtained using the original SSM of (8) to calculate the Voigt function for $x > 75$. In this case, the series number N becomes very large as x increases. The large N costs much CPU time due to the computation of a great number of terms.

The SSM by Limandri can be further improved. Substituting (9) into (8), we obtain a simplified expression of the Voigt function:

$$V(x,y) = \left[\operatorname{erfc}(y)\exp(y^2)\cos(2xy) + \frac{1-\cos(2xy)}{2\pi y}\right]\times\exp\left(-x^2\right) + \frac{2y}{\pi}\sum_{n=1}^{N}V_0(n,x,y) \tag{12}$$

where $V_0(n,x,y)$ is given as

$$V_0(n,x,y) = \frac{\exp[-(x-0.5n)^2]}{n^2+4y^2}\times\left\{\left[\exp(-nx)-\cos(2xy)\right]^2+\sin^2(2xy)\right\} \tag{13}$$

Figure 3 shows the dependence of $V_0(n,x,y)$ on n, wherein $y = 10$ and x is 1.0, 10 and 100, respectively.

It can be seen that the term $V_0(n, x, y)$ reaches its maximal value at neighborhood of $n_0 = \text{int}(2x)$ and it decreases rapidly as n deviates away from n_0. Therefore, in order to save the CPU time, the number of series in the summation $\sum_{n=1}^{N} V_0(n, x, y)$ of (12) may be reduced. Especially, if x is sufficiently large, the summation is not necessary to start from $n = 1$. Instead, it can be replaced by $n = n_0 - n_-$, where n_- is a positive integer less than n_0. Similarly, the end point of the series summation $n = N$ may be replaced by $n = n_0 + n_+$, where n_+ is a positive integer too. Thus, (12) may be rewritten as

$$V(x, y) = \left[\text{erfc}(y)\exp\left(y^2\right)\cos(2xy) + \frac{1-\cos(2xy)}{2\pi y}\right] \times \exp\left(-x^2\right) + \frac{2y}{\pi}\sum_{n=n_{\min}}^{n_{\max}} V_0(n, x, y) \tag{14}$$

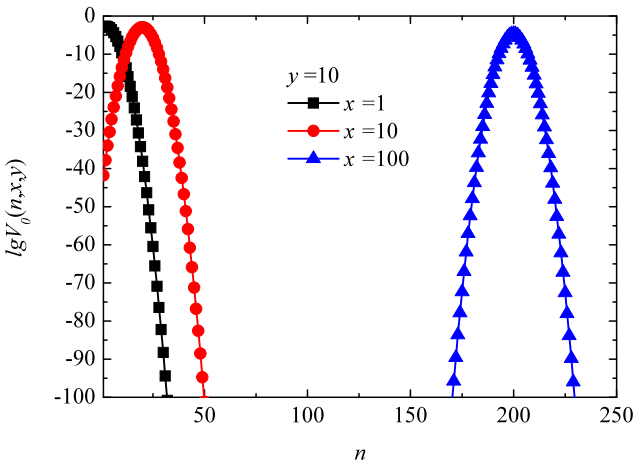

Fig. 3 Dependence of $V_0(n, x, y)$ on n, $y = 10$ and x is 1, 10 and 100, respectively

where the starting point of the series summation is $n_{\min} = n_0 - n_-$ and the end point is $n_{\max} = n_0 + n_+$.

In (13), the factor in the great brackets, i.e. $\{[\exp(-nx) - \cos(2xy)]^2 + \sin^2(2xy)\}$, is approximate to 1. Therefore, we may employ the approximation $V_0(n, x, y) \approx \exp[-(x - 0.5n)^2]/(n^2 + 4y^2)$ to determine the integers n_- and n_+. To do so, we may assume a small value $\varepsilon(> 0)$ and let the equality be

$$V_0(n, x, y) = \varepsilon \cdot V_{0,\max}(n, x, y) \quad \text{where} \quad V_{0,\max}(n, x, y) \approx (n_0^2 + 4y^2)^{-1}. \tag{15}$$

The approximate solution of (15) is obtained as

$$n_- = n_+ = 2\sqrt{-\ln\varepsilon} \tag{16}$$

For example, letting $\varepsilon = 10^{-10}$ then we have $n_- = n_+ = 10$ and hence the starting and the end points of the series summation in (14) are $n_{\min} = n_0 - 10$ and $n_{\max} = n_0 + 10$, respectively. One should pay attention that, when the parameter x is very small, $n_0 - 10$ would be possibly less than 1. In this case, $n_{\min}$ should be equal to 1.

Numerical calculation of the Voigt function is performed using the modified SSM, in which the value of ε is 10^{-10}. To check the accuracy of the numerical calculation, the results obtained with the modified SSM and the original SSM are compared with those published by Zaghloul [18]. The reference values of the Voigt function shown in Table 6 of Ref. [18] are in low relative errors ($<10^{-13}$). In Fig. 4, we provide a comparison between the results of the modified SSM and those of the original SSM, wherein the relative error is defined as the relative difference between the calculated result and the reference value of Ref.18. It can be found that the relative error of the results obtained with the modified SSM is mainly in the order of 10^{-10}. Besides, the results of

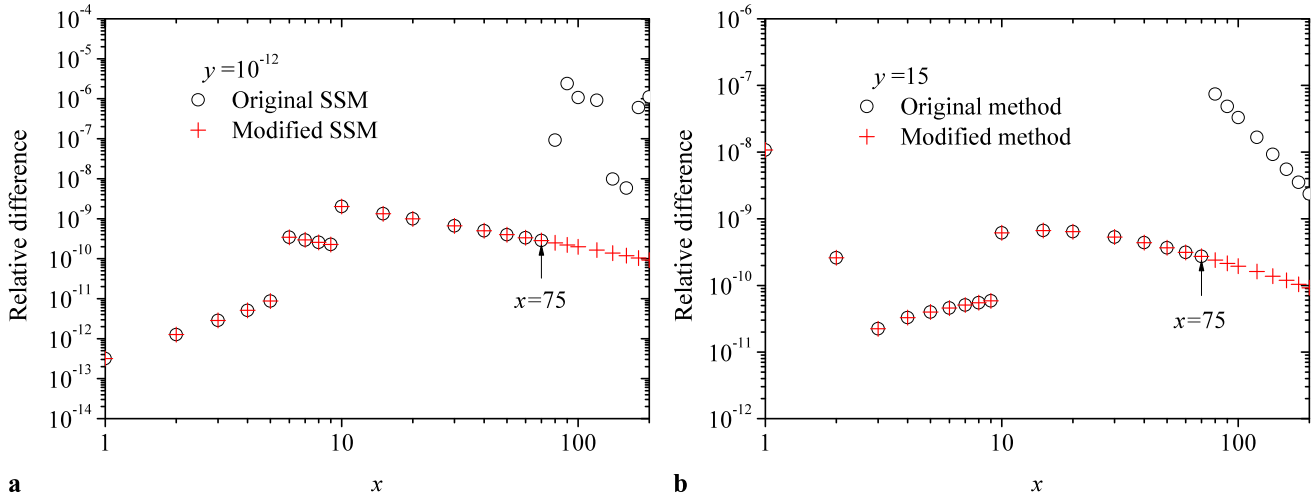

Fig. 4 Relative differences between the results obtained by two series summation methods and those given by Zaghloul for (**a**) $y = 10^{-12}$ and (**b**) $y = 15$

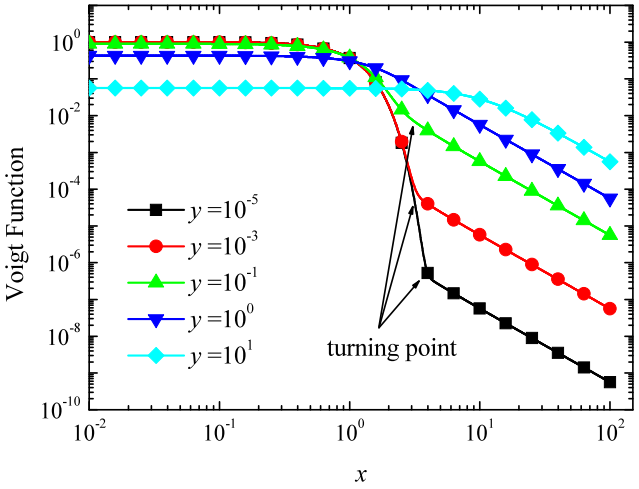

Fig. 5 Numerical results of the Voigt function, $y = 10^{-5}$, 10^{-3}, 10^{-1}, 1 and 10, respectively

the modified SSM coincide with those of the original SSM in the range of $x < 75$. However, visible differences exist in the range of $x \geq 75$. This is because, in the original SSM, the asymptotic expression of (11) is used for $x \geq 75$. Therefore, we may summarize here that the modified SSM is able to give numerical results with the accuracy determined by the value of parameter ε.

An example of the calculation on the Voigt function $V(x, y)$ is shown in Fig. 5 wherein the parameter y is 10^{-5}, 10^{-3}, 10^{-1}, 1 and 10, respectively. It can be found that the Voigt function is of Gaussian profile in the range of small values of x and is of Lorentzian profile for larger x. The turning point depends on the value of y. While $y \ll 1$ (for example $y = 10^{-5}$, 10^{-3} and 10^{-1}), the turning points are quite visible on the curves and it is found that the value of x for the turning point increases as the value of y decreases. However, when y is close to (or larger than) 1, it is difficult to find the turning point. This is because, as y increases, the Voigt function approximates the Lorentzian profile gradually [19].

4 Numerical results and discussions of the PSD

In Sect. 2, we have found an analytical expression of the PSD of the self-mixing signals for the flowing Brownian motion system, which is composed of two Voigt functions. It is well known that the Voigt function is considered a special function itself because the analytical explicit representation in terms of elementary functions does not exist. Therefore, although the dependence of the PSD of the self-mixing signals for the flowing Brownian motion system on the particle size and the flow velocity is involved in the analytical expression, it is difficult to study these relationships quantitatively and instead numerical calculation is performed.

Table 1 The parameters for numerical calculation.

Parameters	Value	Unit
Angle between the scattering vector and flow velocity φ	85	Degree
Beam waist radius ω_0	10	Micrometer
Flow velocity v	0.01	Meter per second
Particle diameter	100	Nanometer
Scattering angle θ	180	Degree
Temperature T	293	Kelven
Viscosity of water η	0.01 @ 293 K	Poise
Wavelength λ	0.6	Micrometer

From Sect. 2, we may find that the PSD of the self-mixing signals possesses a Doppler peak at $\omega = \mathbf{q} \cdot \mathbf{v}$ and the broadening of the power spectral density depends on the combination of the Lorentzian broadening (i.e. $\gamma_L = Dq^2$) and the Gaussian broadening (i.e. $\gamma_G = 2\sqrt{Q \ln 2}$). However, the area beneath the power spectral density is independent of the Lorentzian broadening γ_L and/or the Gaussian broadening γ_G due to the fact that $\int_{-\infty}^{+\infty} S_0(\omega) d\omega = 2\pi$.

In the numerical calculation of the PSD, the values of γ_L, γ_G and $\mathbf{q} \cdot \mathbf{v}$ are estimated with the following relationships:

$$\mathbf{q} \cdot \mathbf{v} = \frac{4\pi v}{\lambda} \sin\frac{\theta}{2} \cos\varphi \tag{17}$$

$$\gamma_L = Dq^2 = \frac{k_B T}{3\pi\eta d} \left(\frac{4\pi}{\lambda} \sin\frac{\theta}{2} \right)^2 \tag{18}$$

$$\gamma_G = 2(Q \ln 2)^{\frac{1}{2}} = \left(\frac{\ln 2}{2} \right)^{\frac{1}{2}} \frac{v \sin\varphi}{\omega_0} \tag{19}$$

The relevant parameters are listed in Table 1. According to these parameters, the values of γ_L, γ_G and $\mathbf{q} \cdot \mathbf{v}$ are 10^3, 10^3 and 10^4 rad/s in order, respectively.

The following figures show the power spectral densities corresponding to different Gaussian or Lorentzian broadening in the case of the scattering vector perpendicular or oblique to the translational velocity of particles.

Figure 6 shows the power spectral densities of the self-mixing signals corresponding to different Lorentzian broadening, while the Gaussian broadening keeps unchanged. In Fig. 6(a), the scattering vector $\mathbf{q}$ is perpendicular to the translational velocity $\mathbf{v}$ of particles. In this case, there is no Doppler shift in the power spectral density because $\mathbf{q} \cdot \mathbf{v}$ is equal to zero. The power spectral densities are dominated by the Gaussian broadening in the range of frequencies close to zero (say $\omega < 6 \times 10^3$ rad s^{-1}) and are dominated by the Lorentzian broadening in the range of high frequencies (say $\omega > 10^4$ rad s^{-1}). As the Lorentzian broadening increases, the power spectral densities in the range of high frequencies shift to much higher frequencies. As compensation, the

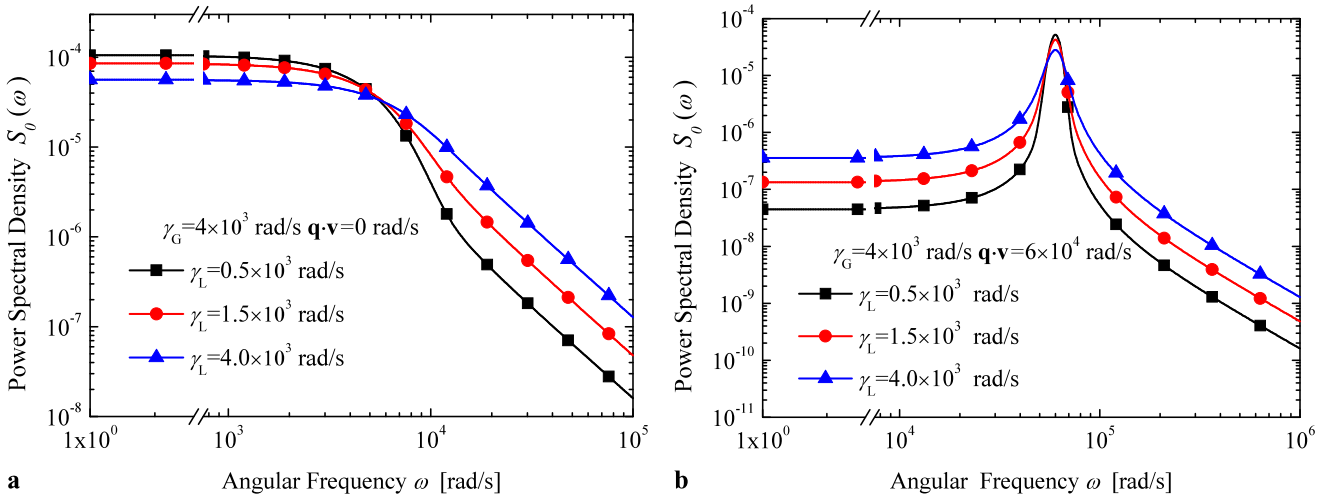

Fig. 6 Power spectral densities of self-mixing signals corresponding to different Lorentzian broadenings: (**a**) without Doppler shift; (**b**) with Doppler shift

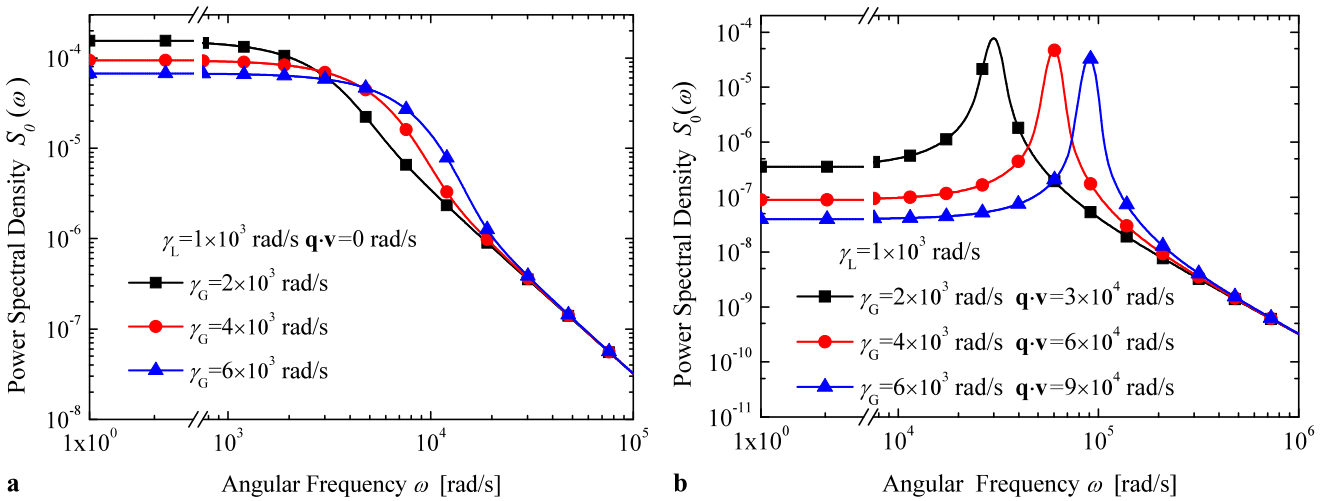

Fig. 7 Power spectral densities of self-mixing signals corresponding to different Gaussian broadenings: (**a**) without Doppler shift; (**b**) with Doppler shift

power spectral densities in the range of low frequencies go down because the area beneath the power spectral densities must keep constant. In Fig. 6(b), the scattering vector is oblique to the translational velocity. In this case, the Doppler peak is located at $\omega = 6 \times 10^4$ rad s^{-1}. The power spectral densities are dominated by the Gaussian broadening in the range of frequencies close to the Doppler peak and are dominated by the Lorentzian broadening in the range of frequencies far away from the Doppler peak. The asymmetry of the curves about the Doppler peak is caused by the sum of the Voigt functions. As the Lorentzian broadening increases, the power spectral densities on the right side of the Doppler peak shift to higher frequencies and the power spectral densities in the range of frequencies close to the Doppler peak go down because of the invariance of the areas beneath the power spectral densities.

Figure 7 shows the power spectral densities of the self-mixing signals corresponding to different Gaussian broadening, while the Lorentzian broadening keeps unchanged. In Fig. 7(a), the scattering vector **q** is perpendicular to the translational velocity **v**. Similarly to Fig. 6(a), there is no Doppler shift in the power spectral density. The power spectral densities in the range of low and high frequencies are dominated by the Gaussian broadening and the Lorentzian broadening, respectively. Since the Lorentzian broadening does not change, the power spectral densities in the range of high frequencies coincide with each other. However, as the Gaussian broadening increases, the power spectral densities

in the range of low frequencies shift to higher frequencies and go down as a compensation (because of the invariance of the areas under the power spectral densities). In Fig. 7(b), the scattering vector is oblique to the translational velocity. In this case, the increase of the Gaussian broadening is necessarily accompanied by the increase of Doppler shift because both of them are related to the translational velocity. As the Gaussian broadening increases by two or three times, the Doppler shift is doubled or trebled. This is because both the Doppler shift $\mathbf{q} \cdot \mathbf{v}$ and the Gaussian broadening γ_G are proportional to the translational velocity, as given in Equations (17) and (19). While the broadening of the power spectral density increases, its height goes down because of the invariance of the areas beneath the power spectral densities.

To summarize, while the scattering vector is perpendicular to the translational velocity, the power spectral density has no Doppler peak. The power spectral density is the convolution of the Gaussian broadening and the Lorentzian broadening. The power spectral density approximates to the Gaussian profile in the range of low frequencies and to the Lorentzian profile in the range of higher frequencies. The Gaussian broadening is related to the translational motion of the particles while the Lorentzian broadening is related to the Brownian motion of the particles. Therefore, information on the translational velocity of particles and the particle size is included in the power spectral density. While the scattering vector is oblique to the translational velocity, the power spectral density has a Doppler shift which is related to the translational velocity of the particles.

The information of the translational velocity of the particles may be obtained either from the Gaussian broadening or from the Doppler peak. In the former case, it is better that the scattering vector is perpendicular to the translational velocity and the Lorentzian broadening very small. That is to say the particle size should be large enough or the translational motion should be very fast so that the Brownian motion can be ignored. In the latter one, the additional information of the angle between the scattering vector and the translational velocity is required. However, it is much easier to find the Doppler peak on the power spectral density.

The information of the particle size is included in the Lorentzian broadening. Unfortunately, for nano-fluids, the Brownian motion is accompanied by translational motion so that the Lorentzian profile is visible only in the range of high frequencies of the power spectral density (or far away from the Doppler peak) and its level is low. So efforts to suppress the Gaussian broadening should be made so as to extract the information of the particle size from the power spectral density. This can be realized by using a wide beam or slowing down the translational velocity. The detailed procedures for extracting the particle size are beyond the scope of this paper and further research on these is required.

5 Conclusions

In this work, we study the power spectral density of the self-mixing signals from a flowing Brownian motion system irradiated by a focused Gaussian field. The power spectral density is derived from the Fourier transform of the time correlation function and composed of two Voigt functions. To calculate the Voigt function much fast and accurately, the SSM is improved. The power spectral densities are calculated, corresponding to different Gaussian or Lorentzian broadening and in the case of the scattering vector perpendicular or oblique to the translational velocity of particle. The numerical results show that, while the scattering vector is perpendicular to the translational velocities of particle, the power spectral density has no Doppler peak and is the convolution of Gaussian broadening and Lorentzian broadening only. The Gaussian broadening is related to the translational velocity of particles and the Lorentzian broadening is related to the particle size. While the scattering vector is oblique to the translational velocity of particle, the power spectral density shows a Doppler peak, which is determined by the translational velocity of particle, the scattering vector and the angle between them. Therefore, the translational velocity can be extracted from the Doppler peak and/or Gaussian broadening, and the particle size can be extracted from the Lorentzian broadening.

Finally, we would point out that in this paper the theory and the numerical calculation are presented for a single particle size and a single flow velocity, while in practice a laminar flowing Brownian motion system contains different sizes of particles and the flow velocity is distributed in a Gaussian profile. Therefore, the power spectral density in a real measurement is much more complicated. The detailed procedures for extracting the particle sizes and flow velocity require the de-convolution of the power spectral density, which is still under investigation.

Acknowledgements The authors acknowledge the support of the National Natural Science Foundation of China (NSFC 50876069), the Specialized Research Fund for the Doctoral Program of Higher Education (SRFDP 20093120110006) and the Fund from the Science and Technology Commission of Shanghai Municipality (No. 10540501000).

References

1. G.H.M. van Tartwijk, D. Lenstra, Quantum Semiclassical Opt. **7**, 87 (1995)
2. N. Sano, Y. Miyasaka, S. Sudo, K. Otsuka, H. Makino, Proc. Schl. Info. Tech. & Electron. Tokai Univ., Ser. E **30**, 33 (2005)
3. S. Sudo, Y. Miyasaka, K. Kamikariya, K. Nemoto, K. Otsuka, Jpn. J. Appl. Phys. **45**, L926 (2006)
4. S. Sudo, Y. Miyasaka, K. Otsuka, Y. Takahashi, T. Oishi, J. Ko, Opt. Express **14**, 1044 (2006)
5. S. Sudo, Y. Miyasaka, K. Nemoto, K. Kamikariya, K. Otsuka, Opt. Express **15**, 8135 (2007)

6. T. Ohtomo, S. Sudo, K. Otsuka, Appl. Opt. **48**, 609 (2009)
7. K. Otsuka, T. Ohtomo, H. Makino, S. Sudo, J. Ko, Appl. Phys. Lett. **94**, 241117 (2009)
8. S. Sudo, T. Ohtomo, Y. Takahashi, T. Oishi, K. Otsuka, Appl. Opt. **48**, 4049 (2009)
9. M. Liu, M. Wang, Proc. SPIE **6830**, 68301C (2007)
10. C. Zakian, M. Dickinson, T. King, J. Opt. A, Pure Appl. Opt. **7**, S445 (2005)
11. C. Zakian, M. Dickinson, T. King, Appl. Opt. **45**, 2240 (2006)
12. H. Wang, J. Shen, Chin. Opt. Lett. **6**, 871 (2008)
13. R. Lang, K. Kobayashi, IEEE J. Quantum Electron. **QE-16**, 347 (1980)
14. H. Wang, J. Shen, B. Wang, B. Yu, Y. Xu, Appl. Phys., B Photophys. Laser Chem. **101**, 173 (2010)
15. S.P. Limandri, R.D. Bonetto, H.O.D. Rocco, J.C. Trincavelli, Spectrochim. Acta, Part B: Atom. Spectrosc. **63**, 962 (2008)
16. W.J. Cody, Math. Comput. **23**, 631 (1969)
17. H.O. Di Rocco, M. AguirreTéllez, Acta Phys. Pol. A **106**, 817 (2004)
18. M.R. Zaghloul, Mon. Not. R. Astron. Soc. **375**, 1043 (2007)
19. G. Pagnini, R.K. Saxena, arXiv:0805.2274v1 (2008)